JOURNAL OF APPLIED PHYSICS **123**, 165101 (2018)

High level active n^+ doping of strained germanium through co-implantation and nanosecond pulsed laser melting

David Pastor,[1,2,a),b)] Hemi H. Gandhi,[1,a),b)] Corentin P. Monmeyran,[3] Austin J. Akey,[4] Ruggero Milazzo,[5] Yan Cai,[3] Enrico Napolitani,[5] Russell M. Gwilliam,[6] Iain F. Crowe,[7] Jurgen Michel,[3] L. C. Kimerling,[3] Anuradha Agarwal,[3,b)] Eric Mazur,[1] and Michael J. Aziz[1,b)]

[1]*Harvard John A. Paulson School of Engineering and Applied Sciences, Cambridge, Massachusetts 02138, USA*
[2]*Departamento de Física Aplicada III, Facultad de Ciencias Físicas, Universidad Complutense de Madrid, Madrid 28040, Spain*
[3]*Massachusetts Institute of Technology, 77 Massachusetts Ave., Cambridge, Massachusetts 02139, USA*
[4]*Harvard Center for Nanoscale Systems, Cambridge, Massachusetts 02138, USA*
[5]*Dipartimento di Fisica e Astronomia, Università di Padova and CNR-IMM, Via, Marzolo 8, Padova I-35131, Italy*
[6]*Ion Beam Centre, University of Surrey, Guildford, Surrey GU2 7XH, United Kingdom*
[7]*Photon Science Institute and School of Electrical and Electronic Engineering, University of Manchester, Manchester M13 9PL, United Kingdom*

(Received 6 November 2017; accepted 17 March 2018; published online 23 April 2018)

Obtaining high level active n^+ carrier concentrations in germanium (Ge) has been a significant challenge for further development of Ge devices. By ion implanting phosphorus (P) and fluorine (F) into Ge and restoring crystallinity using Nd:YAG nanosecond pulsed laser melting (PLM), we demonstrate $10^{20}\,\mathrm{cm}^{-3}$ n^+ carrier concentration in tensile-strained epitaxial germanium-on-silicon. Scanning electron microscopy shows that after laser treatment, samples implanted with P have an ablated surface, whereas P + F co-implanted samples have good crystallinity and a smooth surface topography. We characterize P and F concentration depth profiles using secondary ion mass spectrometry and spreading resistance profiling. The peak carrier concentration, $10^{20}\,\mathrm{cm}^{-3}$ at 80 nm below the surface, coincides with the peak F concentration, illustrating the key role of F in increasing donor activation. Cross-sectional transmission electron microscopy of the co-implanted sample shows that the Ge epilayer region damaged during implantation is a single crystal after PLM. High-resolution X-ray diffraction and Raman spectroscopy measurements both indicate that the as-grown epitaxial layer strain is preserved after PLM. These results demonstrate that co-implantation and PLM can achieve the combination of n^+ carrier concentration and strain in Ge epilayers necessary for next-generation, high-performance Ge-on-Si devices. *Published by AIP Publishing.*
https://doi.org/10.1063/1.5012512

I. INTRODUCTION

Germanium is a promising material platform for the next generation of silicon CMOS-compatible devices. Its high electron and hole mobility, direct (Γ-valley) optical transition at 1.55 μm, and the ability to be directly grown on silicon substrates make Ge attractive for Si integrated electronic and photonic device applications. Ge is becoming a mainstream material—it is already used in commercial telecom photodetectors and will soon be incorporated in high-speed MOSFETs.[1] Promising proof-of-concept Ge IR-emitting lasers[2,3] and LEDs[4,5] were reported recently.

Despite this success, the challenge of obtaining n^+ carrier concentrations from donor doping has been a persistent bottleneck for further development of Ge devices.[6] Large n^+ carrier concentrations are desirable to fabricate ohmic contacts and produce low-parasitic-resistance n-MOSFETS. Additionally, n^+ carrier concentration, in combination with tensile strain, has been shown to facilitate population inversion and lasing emission near 1550 nm.[3,7] Laser gain increases linearly with carrier concentration up to $10^{20}\,\mathrm{cm}^{-3}$.[8] The first electrically pumped Ge lasing proof-of-concept relied on delta-doping to achieve a relatively high n^+ carrier concentration.[3] Since this demonstration, there has been a search for more scalable, lower-cost doping alternatives to achieve even higher n^+ carrier concentrations.[2,9] Conventional *n*-type doping methods, including *in-situ* chemical vapor deposition (CVD) growth,[10–12] gas-phase doping,[13] and ion implantation followed by rapid-thermal annealing (RTA),[14–16] do not yield carrier concentrations greater than $5\times10^{19}\,\mathrm{cm}^{-3}$, regardless of the total chemical donor concentration above this carrier concentration.[6,17] The primary cause of this low active dopant fraction (i.e., carrier to donor concentration ratio) is the ready formation of vacancies and negatively charged donor-vacancy (D-V) clusters that compensate the donor charge.[18–20]

To manage the vacancies and D-V pairs that cause low donor activation, we co-dope epitaxial Ge with phosphorus (P) and fluorine (F). The role of F is to selectively bind to and passivate vacancies that would otherwise bind to P donors and deactivate them. Density functional theory studies suggest that F is effective in passivating vacancies because of the large F-V binding energy, and because its large electronegativity attracts negatively charged vacancies.[21,22] The reason we use P as a donor is that phosphorus-vacancy (P-V) pairs are less likely to associate because they have a lower binding energy

[a)]David Pastor and Hemi H. Gandhi contributed equally to this work.
[b)]Authors to whom correspondence should be addressed: dpastor@fis.ucm.es, hemi.gandhi@gmail.com, anu@mit.edu, and maziz@harvard.edu

than arsenic-vacancy (As-V) and antimony-vacancy (Sb-V) pairs.[23]

Previous P + F co-doping studies were carried out by co-implantation on Ge crystal wafers and Ge-on-Si substrates followed by rapid thermal annealing (RTA),[24,25] but the diffusion of P and F out of the sample during RTA keeps carrier concentrations below n^+ levels. Non-equilibrium, rapid resolidification during pulsed laser melting (PLM) of P-implanted Ge crystal wafers can increase carrier activation to $1 \times 10^{20}\,\mathrm{cm}^{-3}$ levels; however, 20% of donors are still lost due to diffusion in some reports.[26,27] Higher carrier concentrations of up to $2 \times 10^{20}\,\mathrm{cm}^{-3}$ using P donors can be achieved, but demonstrations to date have relied upon complex fabrication procedures involving molecular beam epitaxial growth of P delta-doped multilayers[28] or rear side flash lamp annealing of P-implanted Ge wafers.[29]

In this paper, we use short-pulse PLM on P + F co-implanted strained Ge-on-Si samples, the material platform that will be ultimately used for practical implementation, to obtain crystalline Ge with a high n^+ carrier concentration. Our results show 100% P retention and $10^{20}\,\mathrm{cm}^{-3}$ carrier concentration. Critically, we also show that the short-pulse PLM approach to recover crystallinity and activate the dopants preserves epilayer strain, which is crucial for many device applications.

II. EXPERIMENTAL FABRICATION AND CHARACTERIZATION

We fabricated samples by growing Ge on Si, co-implanting P + F and then laser melting the Ge. We grew a 1-μm Ge epilayer (*in-situ* P doped to $8 \times 10^{18}\,\mathrm{cm}^{-3}$) using a two-step ultrahigh vacuum chemical vapor deposition (CVD) process on a *p*-type (100) Si wafer.[30] The Ge epilayer is strained during growth due to the thermal expansion mismatch between the Ge epilayer and the Si substrate.[30] Next, we implanted one piece of wafer with a 100-keV, 1.85×10^{15}-cm^{-2} P^+ dose. We then treated another piece of wafer with this same 100-keV, 1.85×10^{15}-cm^{-2} P^+ dose and a subsequent 55-keV 1.0×10^{14}-cm^{-2} F^- dose. To restore crystallinity after implantation damage, we then laser-melted each implanted sample with a 355-nm, 0.75-J/cm^2, single 4-ns FWHM pulse from a Nd:YAG laser. We chose this fluence to reach a maximum melt depth (predicted to be 300 nm by numerical solutions[31] to the heat equation in the sample) slightly beyond the 250-nm implant-amorphized region. In this scenario, the melt front reaches the underlying crystalline substrate and leads to single-crystal epilayer regrowth. During PLM of the co-implanted sample, time-resolved reflectivity indicates a melt duration of 85 ns, which is consistent with numerical simulations and suggests that the melt front reaches the expected 300-nm depth.

To characterize surface topography, we imaged the Ge:P and Ge:P + F samples with a high-resolution scanning electron microscope (SEM) before and after PLM. We carried out all subsequent measurements on only the Ge:P + F sample for reasons explained below. To examine the impact of PLM on sub-surface implantation damage, we carried out cross-sectional transmission electron microscopy (XTEM). To measure P and F concentration-depth profiles, we carried out secondary ion mass spectrometry (SIMS). Solecon Laboratories carried out spreading resistance profiling (SRP) measurements to determine the carrier concentration-depth profile. To quantify the effect of PLM on epilayer strain, we carried out high-resolution X-ray diffraction (HRXRD) and Raman spectroscopy measurements. We carried out HRXRD with a parabolic mirror and a Bartels Ge (220) four-crystal monochromator. We selected 8-keV Cu Kα_1 radiation as the probe and reduced the angular acceptance to 12 arc sec by a channel-cut (220) analyzer-equipped detector. We obtained both symmetric (004) and asymmetric (444) reciprocal lattice maps to extract out-of-plane and in-plane sample strain, respectively. For Raman measurements, we used a 532-nm excitation source, focused on a 1-μm spot with a 100× objective lens in a confocal arrangement. We compared room temperature Raman scattering spectra of the laser-melted sample with those of a reference crystalline Ge wafer.

III. DISCUSSION

A. Crystal structure

1. Surface morphology from SEM

Figure 1 shows the surface morphology after PLM of the P-implanted [Fig. 1(a)] and P + F co-implanted samples [Fig. 1(b)]. The P-implanted sample is ablated, whereas the co-implanted sample's surface is smooth and homogeneous. This smoothness indicates that the presence of F suppresses ablation at this fluence. Surprisingly, ablation has not been reported in previous PLM studies of implanted Ge:P crystalline wafers using longer pulse Nd:YAG lasers (12 ns FWHM[32]) or excimer lasers (25–50 ns FWHM).[26,33,34] This

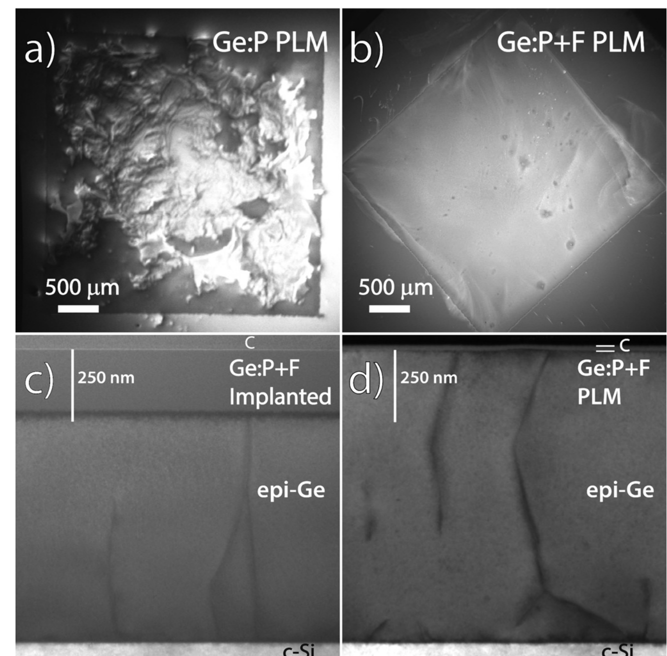

FIG. 1. SEM images of implanted Ge epilayers with (a) 100 keV P at $1.85 \times 10^{15}\,\mathrm{cm}^{-2}$ dose and (b) P (100 keV)+F (55 keV) co-implanted at $1.85 \times 10^{15}\,\mathrm{cm}^{-2}$ and $10^{14}\,\mathrm{cm}^{-2}$ doses, respectively, followed by laser melting at 0.75 J/cm^2. Cross-section TEM micrographs of P + F co-implanted Ge epilayers (c) before and (d) after laser melting at 0.75 J/cm^2.

observation suggests that the shorter 4-ns pulse duration we use plays a role in the ablation. As the ablated P-implanted material is unfit for device fabrication, we carried out all subsequent measurements on only the co-implanted sample.

2. XTEM discussion

Figures 1(c) and 1(d) show XTEM micrographs of the co-implanted sample before and after PLM, respectively. The micrograph of the as-implanted sample shows the 1-μm Ge epilayer atop the crystalline Si substrate. The top 250 nm of this epilayer is amorphous due to P + F implantation damage. Threading dislocations, characteristic of the two-step growth process we used, are visible and arise from the Ge/Si interface.[30] The micrograph of the laser-melted sample indicates that laser melting completely restores the crystallinity of the epilayer after implantation damage, along with the propagation of threading dislocations from the unmelted region to the surface. All examined regions of this sample appear free of residual implantation damage, suggesting that the melt front penetrates through the entire implantation-damaged region.

The threading dislocations visible in the co-implanted sample in Fig. 1(d) likely arise from the epilayer growth process and not from implantation or PLM. No misfit dislocations or stacking faults—which would relax epilayer strain—are visible at the 300-nm melt depth in Fig. 1(d). Furthermore, HRXRD measurements, discussed below, indicate that epilayer strain is preserved after PLM. These observations are consistent with the hypothesis that no new dislocations form after PLM.

B. Dopant and carrier concentrations

1. Dopant concentrations

Figure 2 shows the P-and F-concentration depth profiles from SIMS before and after laser melting. The as-implanted P and F concentration depth profiles each have an expected Gaussian-like shape over the first 250 nm. Both profiles have a peak concentration near 100 nm. At depths beyond the implanted region, both the as-implanted and laser-melted P-concentrations converge to $8 \times 10^{18}\,\text{cm}^{-3}$ (i.e., the as-grown CVD background concentration). The noisy F-concentration signal beyond about 250 nm is a measurement artifact due to the SIMS detection limit near $10^{17}\,\text{cm}^{-3}$. In the laser-melted sample, P-and F-concentration profiles are still Gaussian-like, but have undergone some impurity redistribution compared to the as-implanted profiles. We interpret the surface spike in the laser-melted P profile as a SIMS surface-transient measurement artifact.[35] The P peak is asymmetrically broadened and the peak concentration is slightly reduced. This broadening in P-and F-concentration depth profiles after laser melting is characteristic of liquid-phase impurity diffusion in the melt. The P redistribution we observe is less than previous Ge:P implantation PLM studies using longer pulse lasers.[26,27] We hypothesize that the shorter laser pulse length used here produces a faster solidification front velocity and shorter melt duration, which reduces impurity redistribution after laser melting.

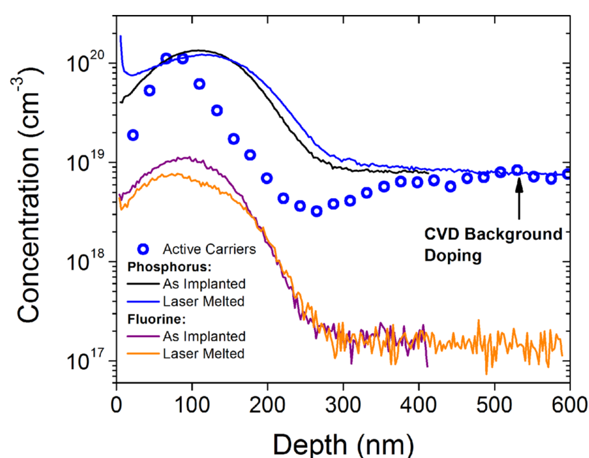

FIG. 2. Solid lines: SIMS P and F concentration-depth profiles obtained from a P + F co-implanted Ge epilayer sample treated identically as in Figs. 1(b)–1(d). Blue circles: SRP carrier concentration-depth profile.

We can estimate the retained impurity-doses after PLM by comparing integrations of the SIMS profiles before and after PLM. For these estimations, we integrate from a depth of 20 nm to 300 nm. We begin integrating from 20 nm because of uncertainty in the SIMS measurement near the sample surface. These integrations indicate that, after PLM, 100% of the P as-implanted dose and around 74% of the as-implanted F dose are retained. While the long-pulse PLM of P-implanted Ge results in 20% P out-diffusion,[26] P + F co-implantation and the short-pulse (4 ns) PLM we carry out here suppress P out-diffusion, even in the absence of a Ge epilayer surface cap.

We explain the loss in the as-implanted F dose after laser-meting as follows. Compared to the as-implanted F-profile, the F-profile of the laser-melted sample has a reduced peak concentration, but no observable distribution broadening or surface accumulation. This observation suggests that the loss of F is caused by out-diffusion and evaporation from the surface during melting. This particular profile, however, would not be expected from simple Fickian diffusion with a sink due to evaporation at the free surface and partitioning at the solidification front.[36] We note that significant F outgassing during solid phase epitaxy is the main challenge in RTA of implanted Ge:P + F.[24]

2. Carrier concentration

Figure 2 also shows the carrier concentration in the laser-melted sample measured by spreading resistance profiling (SRP). We can estimate the fraction of active donors in the laser-melted sample by comparing integrated chemical P (SIMS) and carrier (SRP) concentration curves (integrated from 20–300 m). Assuming that an active P dopant donates one carrier, we obtain an active donor fraction, after PLM, of $44\% \pm 1\%$. More significantly, we note that a peak carrier concentration of $10^{20}\,\text{cm}^{-3}$ is produced at a depth around 80 nm. Interestingly, this peak carrier concentration coincides with the peak F concentration—not the peak P concentration. This observation is consistent with the role of F in increasing the donor activation by passivating vacancies.[21] We note that, at 80 nm depth, where the peak carrier and

peak F concentrations coincide, the donor activation is 100%. At this depth, the coincidence of the peaks, therefore, suggests that the F concentration of $7 \times 10^{18}\,\mathrm{cm}^{-3}$, which is only 7% of the P concentration, is sufficient to passivate all vacancies and produce the observed $10^{20}\,\mathrm{cm}^{-3}$ n^{+} carrier concentration.

Deeper into the sample, the carrier concentration decreases from its peak and reaches a minimum around 260 nm. This minimum carrier concentration is smaller than the as-grown background carrier P concentration (visible beyond around 350 nm). The dip in the carrier concentration is likely due to accumulated point defects, possibly vacancies. Previous studies of laser-melted Si and Ge have observed accumulated vacancies beyond the maximum melt depth.[37,38] It is possible that vacancies beyond the melt depth interact with P and decrease carrier activation in the region with the minimum carrier concentration.

We note that Solecon Laboratories, which performed the SRP measurements and analysis, calculated the carrier concentration assuming the carrier mobility of crystalline germanium wafers.

Solecon Laboratories report an accuracy of ±3% in depth scale, ±15% in resistivity and ±20% in carrier concentration. Solecon Laboratories performed analysis assuming that the sample mobility is that of crystalline Ge wafers. Given that the mobility of the Ge-on-Si sample is likely lower than the literature values for standard Ge crystalline wafers due to residual extended defects from growth, the carrier concentration we report may be slightly underestimated.

C. Strain

1. HRXRD results

Figure 3(a) shows the asymmetric (444) reciprocal space map of the laser-melted sample obtained from HRXRD measurements to investigate sample strain. The dotted full relaxation line consists of coordinates for unstrained, relaxed cubic lattices of varying lattice parameter. Both the measured Ge epilayer and Si substrate peaks are visible in the map. The Ge peak is significantly broadened and displaced from the full relaxation line. This peak broadening is consistent with the presence of epilayer threading dislocations in the sample observed by XTEM. The peak displacement from the full relaxation line indicates tensile biaxial in-plane strain in the epilayer explained as follows. The peak centroid is shifted to a smaller value of $Q_{//}$ as compared to the $Q_{//}$ of fully relaxed, unstrained Ge represented by the red star on the dotted full relaxation line. This peak displacement indicates that the measured Ge has a larger in-plane lattice-constant than unstrained Ge (i.e., it has tensile biaxial in-plane strain). The shift is in the opposite direction for $Q_{\perp}$, indicating that the measured Ge has compressive out-of-plane strain. This reciprocal space map of the laser-melted sample is virtually identical (i.e., no observable change in coordinate peak positions) to the map of the as-implanted sample (not shown). This reciprocal map similarity supports the assertion that epilayer strain is retained after PLM.

The calculated strain values of the as-implanted and laser-melted samples are shown in Table I. We calculate these values from the distances between the Ge and Si peaks along the $Q_{\perp}$ and $Q_{//}$ directions and report the perpendicular ($\varepsilon_{\perp}$) and parallel ($\varepsilon_{//}$) strain with respect to relaxed cubic Ge (lattice constant $a = 0.5658$ nm). The reported strain values are characteristic of epilayer Ge grown from the two-step growth process we use.[39,40] We conclude that the as-grown tensile biaxial in-plane strain of +0.16% is preserved after PLM with an uncertainty of ±0.03%.

The uncertainty in the reported strain values arises because the HRXRD Ge signal originates not just from the laser-melted portion of the epilayer, but from the entire epilayer. The X-rays we use penetrate through the depth of each sample; the recorded Ge signal of scattered X-rays thus emanates from the entire Ge epilayer. The strain values we report, therefore, characterize the average strain of the entire epilayer (i.e., not just the top epilayer portion that has been implanted and/or laser melted). Dislocations create an inhomogenous deformation field that prevents accurate strain depth profiling, which would isolate the strain of the laser-melted epilayer region. However, we can support our conclusion that epilayer strain is preserved after PLM within ±0.03% as follows. We calculate (using the RADS code)[41] that epilayer strain variations larger than ±0.03% in the top 250 nm (i.e., the laser-melted, implanted region), balanced by a corresponding strain variation of opposite sign in the unmelted portion of the Ge epilayer, would split the observed Ge peak under our HRXRD conditions. As we do not observe this peak splitting, we use ±0.03% as an upper limit in the overall uncertainty range in our reported strain values.

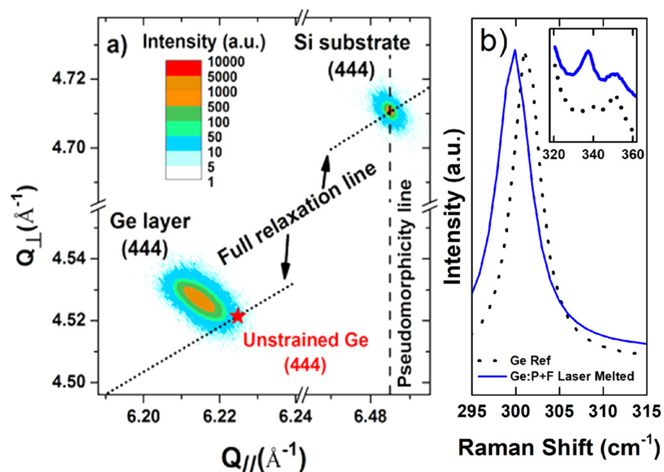

FIG. 3. (a) Asymmetric (444) RSM of the Ge layer and the Si substrate recorded together on implanted samples after PLM at 0.75 J/cm^2. The expected unstrained Ge coordinates are reported as reference. (b) Raman spectra of a reference unstrained, Ge crystal substrate and the Ge:P + F epilayer after PLM at 0.75 J/cm^2. Inset: region around the detected Ge-P local vibrational mode.

2. Raman results

Figure 3(b) shows the normalized Raman spectra of the laser-melted sample and a reference crystalline Ge substrate using a 532-nm probe laser. Considering the absorption coefficient of crystalline Ge[42] at 532 nm ($\alpha = 0.5 \times 10^{6}\,\mathrm{cm}^{-1}$),

TABLE I. Perpendicular and parallel lattice parameters and strain of as-implanted and 0.75 J/cm^2 laser melted samples. The last column reports the change in the unit cell volume with respect to unstrained Ge.

	Symmetric (004)		Antisymmetric (444)		
Sample	$a_{\perp}^{Layer}$ (Å)	$\varepsilon_{\perp}$ (%)	$a_{//}^{Layer}$ (Å)	$\varepsilon_{//}$(%)	$\Delta V/V_{Ge}$ (%)
As implanted	5.6507±0.0001	−0.129±0.002	5.6673±0.0002	+0.164±0.003	+(0.20±0.01)
PLM 0.75 J/cm^2	5.6508±0.0001	−0.129±0.002	5.6671±0.0002	+0.161±0.003	+(0.20±0.01)

we estimate that the Raman signal originates from the top 25 nm of each sample (i.e., from only the implanted and laser-melted portion of the epilayer). The epilayer Raman peak after PLM is red-shifted by about 1 cm^{-1} relative to the unstrained crystalline Ge substrate peak. Using this measured shift and a strain calculation methodology that takes into account Poisson's ratio and the longitudinal and transverse deformation potentials,[43,44] we obtain epilayer tensile biaxial in-plane strain of +0.24%. This qualitatively confirms the presence of tensile strain in the epilayer calculated from HRXRD measurements, although with a magnitude 1.5× large. Considering that the Raman signal probes a small localized region of the epilayer (i.e., the top 25 nm of the epilayer over a 1 μm area laser beam spot size) and that HRXRD probes the entire epilayer (i.e., the entire depth of the epilayer of a wide area of several mm^2), it is possible that the two measurements are not necessarily in disagreement with each other. For example, the Raman measurement possibly probes a localized region not representative of the entire epilayer due to local effects like the presence of dislocations. Because the HRXRD directly measures the lattice spacing over a large area, we believe it as a better probe to deduce the average epilayer strain. The inset of Fig. 3(b) also shows a scattering peak at 337 cm^{-1}, which we attribute to the Ge-P local vibrational mode. This mode corresponds to substitutional P in the Ge lattice; its presence implies that a fraction of the incorporated P is substitutional. This substitutional Raman mode was previously observed in a laser-melted, P-implanted Ge substrate with a 10^{20} cm^{-3} P concentration.[45]

IV. CONCLUSION

In conclusion, we show that short-pulse PLM of P + F co-implanted, strained epitaxial Ge-on-Si can achieve high level n^+ carrier concentrations (10^{20} cm^{-3}) while preserving as-grown strain. The presence of F is associated with the suppression of ablation at the laser fluence we used. After laser melting, the peak carrier concentration coincides with the peak F concentration—not the peak P concentration. This observation is consistent with the current understanding that F increases carrier activation by passivating vacancies that would otherwise bind to and electrically compensate donor dopants. From SIMS data, we estimate that 100% of implanted P is retained after laser melting. XTEM shows that PLM restores epilayer crystallinity after ion-implantation damage. HRXRD measurements demonstrate that PLM preserves the as-grown epilayer strain. HRXRD and Raman measurements both demonstrate the presence of epilayer tensile biaxial in-plane strain after PLM. Raman measurements further indicate that a fraction of the incorporated P atoms occupies substitutional lattice sites. In summary, these results illustrate that P + F co-implantation and short-pulse PLM can achieve the combination of high level active n^+ carrier concentration and strain in Ge epilayers, which represents a major advance for next-generation, high-performance Ge-on-Si devices.

ACKNOWLEDGMENTS

H.H.G. proposed carrying out PLM on P-implanted epilayer Ge-on-Si films to improve carrier activation. I.C. and A.A. suggested the use of F as a co-dopant in this study. Y.C. fabricated the germanium epilayers and performed SRIM simulations at the Massachusetts Institute of Technology's Substrate Engineering Laboratory (SEL) and the Electronic Materials and Devices (EMAT) laboratories, respectively. R.M.G. and I.F.C. performed the ion implantation and initial analysis of implanted material. D.P. performed PLM simulations. D.P. and H.H.G. performed PLM and profilometry. D.P. performed SEM and Raman measurements. C.M. coordinated spreading resistance measurements with Solecon Laboratories Inc. and performed PL and Hall effect measurements (not shown). A.J.A. performed TEM analysis. E.N. performed SIMS measurements. R.M. performed XRD measurements and simulations. H.H.G. and D.P. wrote the first draft of the manuscript under the supervision of M.J.A., E.M., L.C.K, E.N., and A.A. All authors discussed the results and subsequently participated in the revision and approval of the final version of the manuscript. Peter N. Saeta and Alexander Raymond provided feedback on the manuscript.

H.H.G. acknowledges support from the Department of Defense (DoD) under Grant No. DGE 0946799 through the National Defense Science and Engineering Graduate (NDSEG) Fellowship Program and the Directed Energy Processing Society Graduate Fellowship. D.P. acknowledges financial support from the MEC within Programa Nacional de movilidad de recursos humanos del Plan Nacional I+D+i 2008-2011 (No. EX-2010-0662) and to the program Ramón y Cajal (No. RYC-2014-16936). This work was also supported by the U.S. Air Force Office of Scientific Research (No. FA9550-14-1-0150). This work was performed in part at the Harvard Center for Nanoscale Systems (CNS), a member of the National Nanotechnology Infrastructure Network (NNIN), which is supported by the National Science Foundation under NSF Award No. ECS-0335765. This work was also performed in part at the University of Surrey Ion Beam Centre, which is an EPSRC (UK) National Facility. D.P. thanks Mary Gurak for assistance with Raman measurements. C.M., J.M., L.C.K.,

and A.A. acknowledge the support of Defense Threat Reduction Agency (DTRA) Grant No. HDTRA1-13-1-0001. I.F.C. also recognizes the support of MIMIT: Manchester Improving Medicine with Innovation and Technology, as well as the Manchester Academic Health Science Centre (MAHSC).

[1]J. Michel, J. Liu, and L. C. Kimerling, Nat. Photonics **4**, 527 (2010).
[2]J. Liu, X. Sun, R. Camacho-Aguilera, L. C. Kimerling, and J. Michel, Opt. Lett. **35**, 679 (2010).
[3]R. E. Camacho-Aguilera, Y. Cai, N. Patel, J. T. Bessette, M. Romagnoli, L. C. Kimerling, and J. Michel, Opt. Express **20**, 11316 (2012).
[4]S.-L. Cheng, J. Lu, G. Shambat, H.-Y. Yu, K. Saraswat, J. Vuckovic, and Y. Nishi, Opt. Express **17**, 10019 (2009).
[5]M. de Kersauson, R. Jakomin, M. El Kurdi, G. Beaudoin, N. Zerounian, F. Aniel, S. Sauvage, I. Sagnes, and P. Boucaud, J. Appl. Phys. **108**, 023105 (2010).
[6]E. Simoen, M. Schaekers, J. Liu, J. Luo, C. Zhao, K. Barla, and N. Collaert, Phys. Status Solidi A **213**(11), 2799–2808 (2016).
[7]R. Koerner, M. Oehme, M. Gollhofer, M. Schmid, K. Kostecki, S. Bechler, D. Widmann, E. Kasper, and J. Schulze, Opt. Express **23**, 14815 (2015).
[8]X. Sun, J. Liu, L. C. Kimerling, and J. Michel, Appl. Phys. Lett. **95**, 011911 (2009).
[9]R. E. Camacho-Aguilera, Y. Cai, J. T. Bessette, L. C. Kimerling, and J. Michel, Opt. Mater. Express **2**, 1462 (2012).
[10]G. Dilliway, R. V. D. Boom, A. Moussa, F. Leys, B. V. Daele, B. Parmentier, T. Clarysse, E. R. Simoen, C. Defranoux, M. M. Meuris, A. Benedetti, O. Richard, and H. Bender, ECS Trans. **3**, 599 (2006).
[11]H.-Y. Yu, S.-L. Cheng, P. B. Griffin, Y. Nishi, and K. C. Saraswat, IEEE Electron Device Lett. **30**, 1002 (2009).
[12]H.-Y. Yu, E. Battal, A. K. Okyay, J. Shim, J.-H. Park, J. W. Baek, and K. C. Saraswat, Curr. Appl. Phys. **13**, 1060 (2013).
[13]K. Morii, T. Iwasaki, R. Nakane, M. Takenaka, and S. Takagi, in *Proceedings of the IEEE International Electron Devices Meeting (IEDM)* (2009), pp. 1–4.
[14]A. Satta, T. Janssens, T. Clarysse, E. Simoen, M. Meuris, A. Benedetti, I. Hoflijk, B. D. Jaeger, C. Demeurisse, and W. Vandervorst, J. Vac. Sci. Technol. B **24**, 494 (2006).
[15]E. Simoen, A. Satta, A. D'Amore, T. Janssens, T. Clarysse, K. Martens, B. De Jaeger, A. Benedetti, I. Hoflijk, B. Brijs, M. Meuris, and W. Vandervorst, Mater. Sci. Semicond. Process. **9**, 634 (2006).
[16]M. Koike, Y. Kamata, T. Ino, D. Hagishima, K. Tatsumura, M. Koyama, and A. Nishiyama, J. Appl. Phys. **104**, 023523 (2008).
[17]A. Chroneos, J. Mater. Sci.-Mater. Electron. **24**, 1741 (2013).
[18]J. Coutinho, C. Janke, A. Carvalho, V. J. B. Torres, S. Öberg, R. Jones, and P. R. Briddon, Phys. B: Condens. Matter **401–402**, 179 (2007).
[19]A. Chroneos, J. Appl. Phys. **107**, 076102 (2010).
[20]N. S. Patel, C. Monmeyran, A. Agarwal, and L. C. Kimerling, J. Appl. Phys. **118**, 155702 (2015).
[21]A. Chroneos, R. W. Grimes, and H. Bracht, J. Appl. Phys. **106**, 063707 (2009).
[22]A. Chroneos and H. Bracht, Appl. Phys. Rev. **1**, 011301 (2014).
[23]S. Brotzmann and H. Bracht, J. Appl. Phys. **103**, 033508 (2008).
[24]C. Monmeyran, I. F. Crowe, R. M. Gwilliam, J. Michel, L. C. Kimerling, and A. M. Agarwal, Int. Mater. Rev. **62**, 334–337 (2016).
[25]C. Monmeyran, I. F. Crowe, R. M. Gwilliam, C. Heidelberger, E. Napolitani, D. Pastor, H. H. Gandhi, E. Mazur, J. Michel, A. M. Agarwal, and L. C. Kimerling, J. Appl. Phys. **123**, 161524 (2018).
[26]M. Shayesteh, D. O. Connell, F. Gity, P. Murphy-Armando, R. Yu, K. Huet, I. Toque-Tresonne, F. Cristiano, S. Boninelli, H. H. Henrichsen, P. F. Nielsen, D. H. Petersen, and R. Duffy, IEEE Trans. Electron Devices **61**, 4047 (2014).
[27]P. Tsouroutas, D. Tsoukalas, A. Florakis, I. Zergioti, A. A. Serafetinides, N. Cherkashin, B. Marty, and A. Claverie, Mater. Sci. Semicond. Process. **9**, 644 (2006).
[28]G. Scappucci, W. M. Klesse, L. A. Yeoh, D. J. Carter, O. Warschkow, N. A. Marks, D. L. Jaeger, G. Capellini, M. Y. Simmons, and A. R. Hamilton, Sci. Rep. **5**, 12948 (2015).
[29]S. Prucnal, F. Liu, M. Voelskow, L. Vines, L. Rebohle, D. Lang, Y. Berencén, S. Andric, R. Boettger, M. Helm, S. Zhou, and W. Skorupa, Sci. Rep. **6**, 27643 (2016).
[30]H.-C. Luan, D. R. Lim, K. K. Lee, K. M. Chen, J. G. Sandland, K. Wada, and L. C. Kimerling, Appl. Phys. Lett. **75**, 2909 (1999).
[31]LIMP, for Laser Induced Melting Predictions, is the Harvard simulation program provided by Jeffrey West. The original was written by M. O. Thompson and enhanced by J. West, P. M. Smith, and D. Hoglund.
[32]S.-H. Huang, F.-L. Lu, W.-L. Huang, C.-H. Huang, and C. W. Liu, IEEE Electron Device Lett. **36**, 1114 (2015).
[33]C. Wang, C. Li, S. Huang, W. Lu, G. Yan, G. Lin, J. Wei, W. Huang, H. Lai, and S. Chen, Appl. Phys. Express **6**, 106501 (2013).
[34]J. Huang, N. Wu, Q. Zhang, C. Zhu, A. A. O. Tay, G. Chen, and M. Hong, Appl. Phys. Lett. **87**, 173507 (2005).
[35]J. B. Clegg and I. G. Gale, Surf. Interface Anal. **17**, 190 (1991).
[36]B. P. Bob, A. Kohno, S. Charnvanichborikarn, J. M. Warrender, I. Umezu, M. Tabbal, J. S. Williams, and M. J. Aziz, J. Appl. Phys. **107**, 123506 (2010).
[37]T. Kalliovaara, J. Slotte, I. Makkonen, J. Kujala, F. Tuomisto, R. Milazzo, G. Impellizzeri, G. Fortunato, and E. Napolitani, Appl. Phys. Lett. **109**, 182107 (2016).
[38]G. Mannino, V. Privitera, A. La Magna, E. Rimini, E. Napolitani, G. Fortunato, and L. Mariucci, Appl. Phys. Lett. **86**, 051909 (2005).
[39]G. A. Slack and S. F. Bartram, J. Appl. Phys. **46**, 89 (1975).
[40]Y. Ishikawa, K. Wada, D. D. Cannon, J. Liu, H.-C. Luan, and L. C. Kimerling, Appl. Phys. Lett. **82**, 2044 (2003).
[41]M. Wormington, C. Panaccione, K. M. Matney, and D. K. Bowen, Philos. Trans. R. Soc. Math. Phys. Eng. Sci. **357**, 2827 (1999).
[42]H. R. Philipp and E. A. Taft, Phys. Rev. **113**, 1002 (1959).
[43]B. S.-I. Pearson, "Germanium photodetectors on amorphous substrates for electronic-photonic integration," Ph.D. thesis (Massachusetts Institute of Technology, 2016).
[44]Y.-Y. Fang, J. Tolle, R. Roucka, A. V. G. Chizmeshya, J. Kouvetakis, V. R. D'Costa, and J. Menéndez, Appl. Phys. Lett. **90**, 061915 (2007).
[45]G. Contreras, A. Compaan, and A. Axmann, J. Phys. Colloq. **44**, C5-193–C5-195 (1983).